Ultrafast Harmonic Mode-Locking of Monolithic Compound-Cavity Laser Diodes Incorporating Photonic-Bandgap Reflectors

Dan A. Yanson, Michael W. Street, Stewart D. McDougall, Iain G. Thayne, *Member, IEEE*, John H. Marsh, *Fellow, IEEE*, and Eugene A. Avrutin, *Member, IEEE*

***Abstract*—We present the first demonstration of reproducible harmonic mode-locked operation from a novel design of monolithic semiconductor laser comprising a compound cavity formed by a 1-D photonic-bandgap (PBG) mirror. Mode-locking (ML) is achieved at a harmonic of the fundamental round-trip frequency with pulse repetition rates from 131 GHz up to a record high frequency of 2.1 THz. The devices are fabricated from GaAs–AlGaAs material emitting at a wavelength of 860 nm and incorporate two gain sections with an etched PBG reflector between them, and a saturable absorber section. Autocorrelation studies are reported which allow the device behavior for different ML frequencies, compound cavity ratios, and type and number of intra-cavity reflectors to be analyzed. The highly reflective PBG microstructures are shown to be essential for subharmonic-free ML operation of the high-frequency devices. We have also demonstrated that the single PBG reflector can be replaced by two separate features with lower optical loss. These lasers may find applications in terahertz imaging, medicine, ultrafast optical links, and atmospheric sensing.**

***Index Terms*—Microwave generation, mode-locked lasers, optical modulation, optoelectronic devices, quantum-well lasers, semiconductor lasers, submillimeter wave generation, submillimeter wave modulation.**

I. Introduction

THE GENERATION of power at terahertz frequencies has been attracting much interest in recent years, with applications in millimeter-wave imaging, radio astronomy, and atmospheric sensing. In medicine, for example, terahertz imaging can potentially supersede X-rays as a safe diagnostic tool. However, few sources exist that cover this spectral region, with their available average powers limited to microwatts. As a promising way forward, optical methods of terahertz generation are currently being pursued. Optical input can be downconverted into the microwave domain by optical heterodyning or photomixing [1], [2], which involves coupling light from two wavelength-offset laser sources into a specially designed fast photoreceiver, such as a low-temperature grown GaAs detector with an integrated terahertz antenna, to produce radiation at the difference terahertz frequency. The photomixing scheme may be potentially both simplified and improved by replacing the two lasers with a single optical source generating a comb of narrow-linewidth, equidistant modes offset by the required terahertzfrequency—such as an ultrafast ML laser. Such a laser can also be used as a local oscillator source in terahertz measurement and diagnostics applications, e.g., in superheterodyne detection, whereby an incoming terahertz signal of interest can be mixed directly with the optical output of a ML laser to generate a beating envelope which can be readily measured with conventional electronics. Ultimately, it has been suggested that such mixing can be performed within the saturable absorption section of the laser itself [3]. An overview and analysis of ultrafast ML techniques for semiconductor lasers can be found in [4].

Semiconductor lasers offer higher ML frequencies than any other type of laser, by virtue of their short cavity length. However, practical constraints on the cavity length limit the fundamental repetition frequencies to around 240 GHz [5]. Higher pulse-repetition rates can be achieved with a method known as harmonic ML. A harmonic ML laser produces an optical pulse train at a harmonic of the fundamental round-trip frequency, which can be achieved with either of two main techniques: colliding pulse ML (CPM), including multiple [6] and asymmetric [7] CPM, and compound-cavity ML (CCM). The (asymmetric) CPM effect has been used to obtain ML at repetition frequencies up to 860 GHz [7]. Frequencies of up to 1.5 THz have been achieved with the use of a version of the CCM effect in DBR lasers [8]—but in a construction not intended specifically for harmonic ML, under a narrow range of operation conditions and with limited reproducibility. Here, we report reproducible harmonic ML operation at 2.1 THz from what is, to our knowledge, the first purpose-fabricated monolithic CCM laser diodes, based on a construction proposed theoretically in [4], [9], [10].

The structure of the paper is straightforward. Section II summarizes the theoretical basis for the device operation principle. Section III addresses the design and fabrication issues. Section IV presents the experimental methodology, and in Section V, the experimental results obtained are presented and compared with the theoretical predictions. Section VI states the conclusions.

II. Theory

The theory of CCM we use here is a slight extension of the approach developed in earlier work [9], [10]. We use the time-fre-

Manuscript received June 12, 2001; revised October 2, 2001.

D. A. Yanson, M. W. Street, S. D. McDougall, I. G. Thayne, and J. H. Marsh are with the Optoelectronics Research Group, Department of Electronics and Electrical Engineering, University of Glasgow, Glasgow G12 8LT, U.K. (e-mail: yanson@elec.gla.ac.uk).

E. A. Avrutin is with the Department of Electronics, University of York, York YO10 5DD, U.K. (e-mail: eaa2@ohm.york.ac.uk).

Publisher Item Identifier S 0018-9197(02)00173-2.

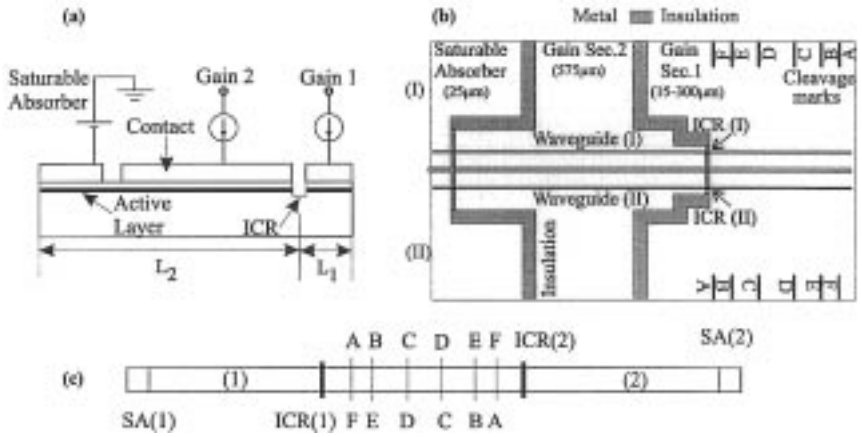

Fig. 1. Schematic of a monolithic CCM device with an etched ICR. (a) Cross-section and pumping arrangement. L_1/L_2 defines the optical cavity ratio created by ICR. (b) Plan view showing two symmetric devices on one chip with different ICRs. (c) Reciprocal device layout allowing two lasers with exact $1/m$ and $1/n$ cavity ratios to be cleaved simultaneously at any of the points A–F.

quency domain model [11], [23] based on decomposition of the lasing light in terms of longitudinal modes of the active cavity:

$$E(r,\,t) = \Phi(x,\,y)\sum_k \mathrm{E}_k(t)u_k(z)\exp(i\omega_k t) \tag{1}$$

where Φ is the profile of the (single) transverse-lateral mode, and

$$\mathrm{E}_k(t) = E_k(t)e^{i\varphi k^{(t)}} \tag{2}$$

represents complex modal amplitudes (with E. φ is the real amplitude and phase, respectively), $u_k(z)$ is the instantaneous mode profiles, and ω_k is equidistant frequencies. The time evolution of the complex-mode amplitudes is then governed by

$$\frac{d}{dt}\mathrm{E}_k(t) \approx [\gamma_k + i(\Omega_k - \omega_k)]\mathrm{E}_k(t) + \sum_{m\neq 0} G_m(t)\mathrm{E}_{k-m}(t). \tag{3}$$

Here, the parameter γ_k is the effective (amplitude) net gain of the kth mode and Ω_k is the cold-cavity (i.e., calculated for uncoupled modes) modal frequency. The parameters G_m (for full expressions, see [4], [6], [11], [23]) are responsible for passive ML and describe the strength of the interaction, via net gain pulsations caused by mode beating, between modes that are m fundamental modal intervals apart. The general formalism (1)–(3) applies to a broad variety of laser structures [4], [11], [23], with a structure's geometry entering the model via the mode-coupling parameters G_m and the modal eigenvalues

$$\delta_k = \Omega_k - i\gamma_k. \tag{4}$$

Here, we shall specifically consider a CCM laser [Fig. 1(a)] with an intra-cavity reflector (ICR) separating the cavity of length L into two sub-sections of length $L_{1,2} = f_{1,2}L$, with $f_2 = 1 - f_1$. The longer subsection 2 includes a saturable absorber of length $L_a = f_a L$, the remaining length $L_{g2} = f_{g2}L = L_2 - L_a$ being forward biased (amplifying). Then, it is convenient to write

$$2\gamma_k = (f_1 g_1 + f_{g2} g_2 - f_a a - (a_i + a_{ck})). \tag{5}$$

Here, $g_{1,2}$ and a are the gain/saturable absorption coefficients (the weak k-dependence due to material gain dispersion is omitted for simplicity), $f_{1,g2,a}$ are the length fractions of the corresponding sections, and a_i and a_{ck} are, respectively, the internal and outcoupling losses for each mode. It is the latter parameter that predominantly determines the harmonic operation of the CCM laser—the dependence of a_{ck} on k favors a fixed set of modes (those with the lowest losses) in the lasing spectrum. (As noticed earlier [10], this predominantly linear selectivity mechanism is rather different from the situation in multiple and asymmetric CPM constructions—there, the selectivity is provided solely by the nonlinear mode interaction parameters G_m so that the cavity geometry determines just the harmonic number, not the actual lasing modes, leading to an increased risk of supermode competition). It is therefore useful to discuss the modal loss properties of CCM lasers in some more detail.

Generally speaking, (5) for the net modal gains γ_k should be used with some care, since the outcoupling losses a_{ck} may themselves depend on gain and saturable absorption (and be, therefore, parametrically time-dependent), particularly due to the carrier-density-dependent refractive index. Most generally, γ_k should be calculated directly from the complex modal eigenvalues δ_k (4). To find these eigenvalues (and, by the same token, the mode profiles u_k), we follow the procedure commonly used for threshold loss analysis in complex laser cavities. We express the mode profiles as linear combinations of forward- and backward-propagating waves with complex wave vectors

$$q_{g1(2)k} = \delta_k + 1/2(-ig_{1(2)} + g''), \quad q_{ak} = \delta_k + 1/2(ia + a'') \tag{6}$$

inside the gain and SA sections respectively, with g'' and a'' describing the optical frequency chirp due to the carrier-density-dependent refractive index associated with gain g and saturable absorption a. We then require that these waves satisfy the usual reflectance/transmittance boundary conditions at the facets and the intermediate reflector, the latter being assigned phenomenological (amplitude) transmittance and reflectance coefficients t_{ICR} and r_{ICR}. This procedure yields a transcendental equation for δ_k

$$\delta_k = \delta_k^{(0)} + \frac{i}{2L}\log[(1 - r_{\mathrm{ICR}}r_1\exp(-i2q_{g1k}L_1)) \times (1 - r_{\mathrm{ICR}}r_2\exp(-i2q_{g2k}L_{g2} - i2q_{ak}L_a))] \tag{7}$$

where $r_{1,2}$ are the *amplitude* reflectances of facets bordering the corresponding sections. Equation (7) is a generalization of formulae used in the literature for cleaved-coupled-cavity lasers (see below); here, it is written in such a form that the first term

$$\delta_k^{(0)} = \frac{\pi k}{L} + \frac{1}{2}\left(f_a a'' + f_1 g_1'' + f_{g2} g_2''\right) + \frac{i}{2}\left[\ln\frac{1}{r_1 r_2 t_{\rm ICR}^2} + f_a a - f_1 g_1 - f_{g2} g_2\right] \quad (8)$$

describes the solution for a simple, unperturbed Fabry–Pérot cavity, whilst the second term contains the effect of intermediate reflectance. This is particularly convenient in the (practically quite common) case of small ICR reflectance $r_{\rm ICR} \ll 1$,, $t_{\rm ICR} \approx 1$, which results in relatively small differences between mode output losses. Then, (7) is easily simplified [10] and may, indeed, be written in the form of (5), in which the values of cavity losses a_{ck} do not depend explicitly on gain/saturable absorption and may be estimated from a simple approximation

$$a_{ck} = \frac{1}{L}\ln\frac{1}{r_1 r_2} + \Delta a_{ck}$$
$$\Delta a_{ck} \approx -\frac{r_{\rm ICR}}{L}\left(\frac{r_1^{f_2}}{r_2^{f_1}} + \frac{r_2^{f_1}}{r_1^{f_2}}\right)\cos(2\pi f_1 k) \quad (9)$$

(more precisely, the fraction of the *optical*, rather than geometrical, length of the shorter subcavity should be used in the argument of the cosine).

The cosine in expression (9) reaches its maximum value of one for certain discrete mode numbers k, separated by a multiple of $M = 1/mf_1$, M and m being integers. With every Mth mode having a minimum loss, mode locking is predicted at the Mth harmonic whenever the sub-cavity length ratio $L_1 : L_2 = m : n$ with $M = m + n$ for integer m and n. More specifically, when $m = 1$, $L_1 : L_2 = 1 : (M-1)$. In both the general $(m : M-m)$ and the specific $(1 : M-1)$ cases, all but every Mth mode have a higher loss and are therefore suppressed in the lasing output. The harmonic ML frequency is $f = Mf_F$, f_F being the fundamental ML frequency. In spectral terms, this corresponds to an M-fold multiplication of the mode separation in the lasing spectrum, $\Delta\Lambda_{CCM} = M\,\Delta\lambda_{F-P}$, ($\Delta\lambda_{F-P}$ is the cavity's Fabry–Pérot mode spacing). The harmonic mode spacing is effectively that of the shorter sub-cavity, as is the ML frequency. The exact degree to which all nonharmonic modes are suppressed is determined by the cavity discrimination, which can be quantified as the smallest loss difference between a harmonic mode and a nonharmonic one. In the special $(1 : M-1)$ case, the discrimination is given by

$$\delta a_c = a_{c1} - a_{c0}. \quad (10)$$

In the case of $r_{\rm ICR} \ll 1$, the selectivity δa_c is defined by (9) and is thus proportional to $r_{\rm ICR}$. In the general case, (7) has to be solved numerically. At $R_{\rm ICR} = r_{\rm ICR}^2 \sim 0.001$–$0.01$, the linear dependence of δa_c on $r_{\rm ICR}$ (9) holds well. A further increase in the intermediate reflection continues to improve the selectivity (in accordance with our numerical time-domain simulations [12], which predicted more reliable harmonic operation

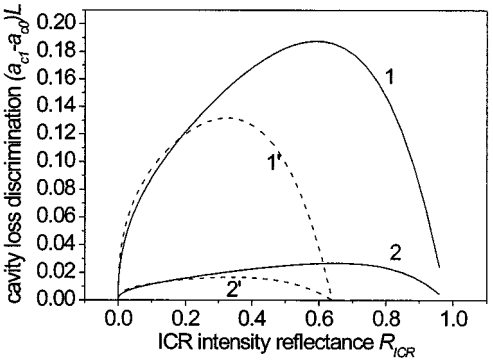

Fig. 2. Calculated selectivity of the harmonic cavity versus ICR reflectance. ICR position $f_1 = 1/M = 1/11\,(1,\,1')$ and $1/30\,(2,\,2')$. Solid curves $(1, 2)$: $r_{\rm ICR}^2 + t_{\rm ICR}^2 = 1$ (no scattering or losses at ICR); dashed curves $(1', 2')$: $r_{\rm ICR}^2 + t_{\rm ICR}^2 = 0.64$.

with shorter pulses in lasers with highly reflective microstructures used as ICRs). However, the rate of selectivity improvement slows down considerably, and at $R_{\rm ICR} \sim 0.6$–0.9, δa_c shows a broad peak and then falls as $r_{\rm ICR}$ approaches unity (with losses and scattering at the ICR taken into account by setting $R_{\rm ICR} + t_{\rm ICR}^2 < 1$, the maximum shifts to lower reflectances). This implies that there is a limit to the improvement of the quality of harmonic ML through the use of highly reflective ICRs. Unsurprisingly, (7) and (9) predict that the maximum cavity selectivity achievable with a single reflector falls drastically with the harmonic number M. In a particular case where the sub-section ratio is $(1 : M-1)$ and $M = 1/f_1$, the series decomposition of the cosine term in (9) in the limit of $kf_1 = k/M \ll 1$, gives for large M an estimate

$$\delta a_c \approx -\frac{2r_{\rm ICR}}{L}\left(\frac{r_1^{f_2}}{r_2^{f_1}} + \frac{r_2^{f_1}}{r_1^{f_2}}\right)\left(\frac{\pi}{M}\right)^2.$$

The calculations presented in Fig. 2 have been performed for $g_1 = g_2 = -a$, i.e., for a cavity homogeneously pumped below threshold. The selectivity δa_c can be increased by preferentially pumping the shorter subsection to ensure $g_1 > g_2$. However, as long as $g_1 L \ll M$ and/or $r_{\rm ICR} \ll 1$ (i.e., neither section approaches lasing individually), this improvement remains modest. Within these limits, we also found that the dependence of the mode losses a_{ck} (and hence of δa_c) on g_1, g_2, and a is nearly linear, as in (5), which speeds up the numerical integration of (3).

An alternative method of improving mode selectivity at high M is then to use more than one ICR, as was done in [16] to achieve single-frequency lasing. Whilst the general expression for the modal loss a_{ck} in the case of two or more ICRs is very cumbersome, in the case of $r_{\rm ICR} \ll 1$, the contributions from individual reflectors to Δa_{ck} can be treated additively, with each individual term calculated via (9). Particularly promising is the use of two reflectors positioned at different fractions of the cavity length, as each of them is then responsible for suppressing a different subset of "nonharmonic" modes, leading to a much stronger overall selectivity. The first slot, which divides the cavity into an m, n ratio, provides suppression for the Fabry–Pérot modes nearest to the harmonic modes, whereas the second slot at a ratio of $1 : k$ offers discrimination against the

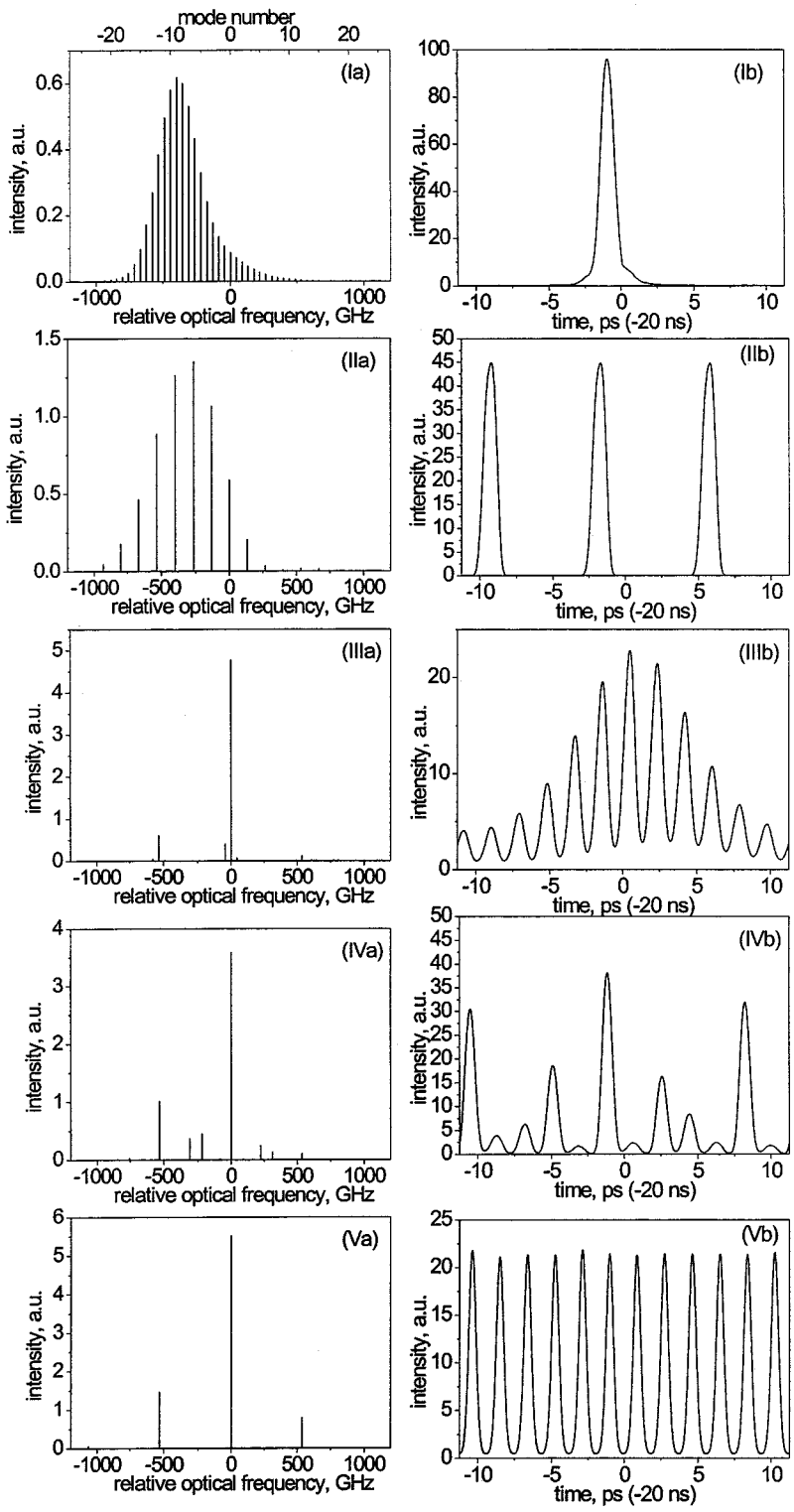

Fig. 3. (a) Typical simulated lasing spectra and (b) corresponding pulse trains for a laser with $L = 900\,\mu$m (fundamental repetition rate = 44 GHz) and $L_a = 30$ μm. (I) Fundamental frequency ML with no ICRs. (II) Harmonic ML ($M = 3$) with an ICR at $L/3$. (III–IV) Incompletely rendered harmonic ML ($M = 12$) with single ICRs at $L/12$ (III) and $5L/12$ (IV). (V) Good quality harmonic ML ($M = 12$) with the combined effect of two ICRs at $L/3$ and $5L/12$. Assumed $R_{\mathrm{ICR}} = 0.01$.

fundamental modes located toward the middle of the intervals between the adjacent harmonic modes (here, m, n, and k are integers without common factors). With $(m+n)$ being equal to or a multiple of $(1+k)$, both ICRs will select the same harmonic $M = m + n$, one ICR complementing the spectral selectivity of the other.

The above considerations are further illustrated by the simulated lasing spectra of Fig. 3(a) obtained by full numerical so-

lution of complex rate equations (3) complete with rate equations for the carrier density in the gain and saturable absorber sections [11], [23]. The method has been demonstrated [11], [23] to give good agreement, for different laser structures, with the more generic but much slower distributed time-domain approach that we used in our earlier work, which allows us to use a single model throughout the present study without recourse to distributed time-domain modeling. The graphs of Fig. 3(b) have been produced by summation of the Fourier series (with modal phases provided by calculations along with the amplitudes) and represents a fragment of the pulse train within the timeframe of a single round-trip of the long cavity, registered at 20 ns after turn-on to allow the transients to settle down. The geometry of the laser approximates that of a fabricated device (see Section V below), and the parameters of the material were chosen within the limits quoted in literature and are similar to those used in earlier work [6], [9], [11], [23]. In the case of an unperturbed cavity with no ICR, Fig. 3(I), the usual picture of fundamental frequency ML is simulated, with the spectrum being shifted and asymmetric due to self-phase modulation. A single ICR at 1/3 of the cavity length, with an intensity reflectance of $R_{\mathrm{ICR}} = 0.01$, provides a very good quality third harmonic ML shown in Fig. 3(II) (the intermediate modes for this value of R_{ICR} are suppressed by over 60 dB). However, for a higher harmonic number of $M = 12$, the selectivity of a single reflector is insufficient to achieve uniform harmonic operation in the relatively long cavity, whether the ICR is positioned at 1/12 [Fig. 3(III)] or 5/12 [Fig. 3(IV)] of the cavity length. Nonetheless, the combined effect of two identical ICRs, in this case at $L/3$ and $5L/12$, clears the spectrum of intermediate modes resulting in good quality harmonic ML with $M = 12$ [Fig. 3(V)]. This is due to the fact that both ICRs simultaneously select every 12th mode only.

III. Design and Fabrication

A. Background and Technology

The fabricated CCM devices are similar to "C^3" (cleaved coupled-cavity) lasers [13], except that they are monolithic, with an ICR defined by dry-etching, and contain an additional contact section (saturable absorber), which is required for ML operation. The C^3 devices were regarded as the "poor man's DFB laser" of the 1980s, as they could operate single-mode with a side-mode suppression ratio of 20–35 dB without the expense of a DFB grating. However, they were plagued with alignment and reliability problems due to the inherent inability to maintain a constant gap between the two sub-cavities. The monolithic approach, by contrast, is less prone to stability problems as it keeps the original waveguide alignment intact, whilst relying on nonmechanical techniques to create a compound cavity. Early attempts included the definition of etched ICRs by reactive ion etching [14], laser ablation [15] and, more recently, focused ion beam etching [16], which was particularly successful in obtaining reliable single-mode operation by carefully controlling the ICR position and size with minimum threshold penalty. In [16], single and multiple ICRs were employed to modify the Fabry–Pérot spectrum by "mode sculpturing," with the typical ICR reflectivity between 10^{-3} and 10^{-2}. With a different task in mind, we used the "mode sculpturing" methodology of [16] to obtain desired spectral transformations, with ICRs defined by more mature reactive ion etching technology than that used in [14]. However, early trials showed that much more reflective ICRs are required if these compound-cavity lasers are to be ML, especially at higher harmonics. We have, therefore, created a compound cavity with the use of 1-D photonic bandgap (PBG) mirrors [17], [18] formed by a series of deep-etched sub-wavelength slots, with reflectivities approaching 80%.

B. Material and Fabrication

With a proof-of-principle demonstration in mind, we have chosen to fabricate the CCM lasers in a GaAs–AlGaAs double quantum-well structure operating at $\lambda = 860$ nm (the wavelength is of relatively low importance for most of the proposed applications). This material system offers the most mature growth and processing technology, as well as ease of fabrication. The epilayer used was a separate confinement heterostructure grown by MOCVD on a doped GaAs substrate, with two 10 -nm-wide GaAs quantum wells buried 1 μm from the surface. The devices were essentially three-section ridge-waveguide laser diodes, incorporating a saturable absorber and two gain sections with an etched ICR between them. The cross-section of a complete device and the pumping arrangement are illustrated in Fig. 1(a). The possibility to pump the device differentially through the *Gain 1* and *Gain 2* enables a good match with the target sub-cavity ratio by fine-tuning the optical resonator lengths, and can also potentially improve the cavity selectivity, as discussed earlier (Section II).

The basic fabrication process involved the patterning and dry-etching of 3-μm-wide waveguide ridges, p-contact deposition and lift-off, followed by wafer thinning and n-side metallization and annealing. All lithography steps were direct written by a LEICA Beamwriter (EPBG-5HR) to allow the sub-micron ICR features to be accurately defined. Four types of ICR have been fabricated, which are, in order of decreasing reflectivity: a short third-order PBG mirror of four deep 100–nm slots [see photograph of Fig. 7(I-a)], a single 200–nm wide slot [Fig. 7(II-a)], a shallow 400–nm slot [Fig. 7(III-a)], and a shallow 13-period first-order grating (not shown). In the first two cases, the slots were etched through the active layer to a depth of $\sim 1.5 \div 2\ \mu$m, which was done prior to waveguide definition using an SiO_2 mask and reactive ion etching with $SiCl_4$ and a fraction of O_2 (the oxygen was added to improve sidewall verticality in the slots, see [18]). On the other hand, the shallow slots and gratings were defined and etched concurrently with the 0.6 μm tall waveguides, using the same process without O_2. Some shallow slots were later re-opened for p-contact deposition, with a view to increasing their reflectivity by filling them up with metal. This, however, had little effect on the device performance.

To allow direct comparison between different types of ICR, two symmetric lasers with different ICRs (or with one having none at all) were placed on a single chip, with the two waveguides electrically and optically isolated from each other by a 50 -μm gap, as shown in Fig. 1(b). Since both lasers were cleaved to precisely the same length, we were able to evaluate the difference between each type of ICR and/or the unperturbed waveguide with all other parameters identical.

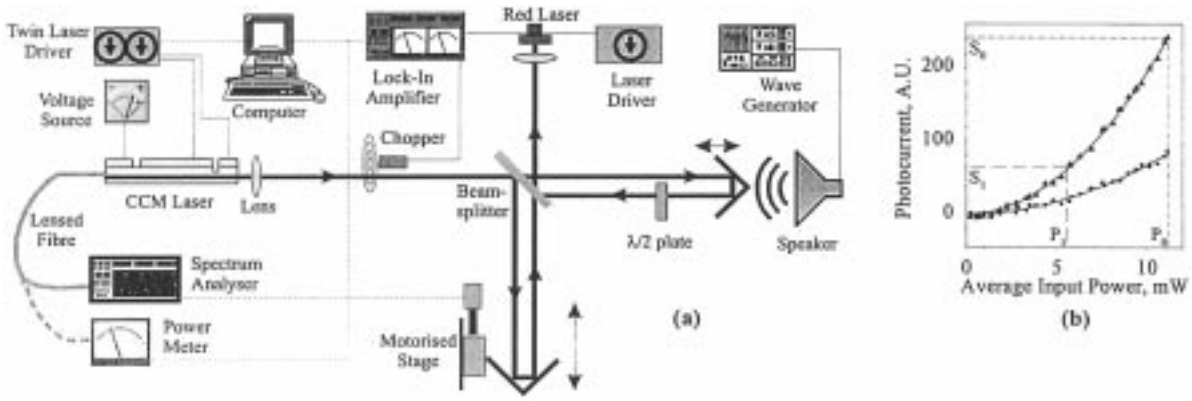

Fig. 4. (a) Diagram of experiment setup allowing simultaneous spectrum and autocorrelation measurements. (b) Response of the nonlinear two-photon absorption detector (red laser) where the source laser is modelocked and unlocked (upper and lower curves, respectively). The ML data is fitted with a parabola (thin line) $S = \alpha P + \beta P^2$, with $\beta/\alpha^2 \sim 4.8$. In autocorrelation data, the contribution of linear absorption αP was cancelled out by calibrating the signal at points P_0 and $P_1 = P_0/2$.

The devices were laid out in such a way that the length of the longer sub-cavity was kept constant at 600 μm, whilst the length of the shorter one was varied from 300 μm down to 15 μm, resulting in sub-cavity ratios from 1 : 2 to 1 : 40 (with design harmonics $M = 3$–41). Note that multiplication of the absolute repetition frequency is achieved both by an increased harmonic number through more asymmetric ratios and the reduction of the total cavity length. A reciprocal device layout was designed with two devices facing each other [see Fig. 1(c)], so that when one was cleaved to length A (implying a given $1 : m$ ratio), the other would be automatically cleaved to length F (with different $1 : n$ ratio), the next pair being lengths B and E, etc. Ratios of the generic $m : n$ type could be obtained by deviating from the designated cleavage markers A–F.

Accurate sub-cavity length ratios are essential if harmonic effects are to occur in CCM lasers [9], [10]. They are particularly important in high-harmonic devices, where an error of only a few microns can result in ML at a different harmonic. However, the accuracy of the conventional wafer scriber used to cleave the devices proved insufficient, and a special, wet-etch facilitated cleaving process was developed. This involved the use of a fast anisotropic etch ($H_2SO_4 : H_2O_2 : H_2O$ with volume parts 1 : 8 : 40) to produce ~70-μm-deep triangular nicks from lithographically defined 2-μm-wide seed windows along the sample edge. The total device length error was of the order of ± 6 μm.

Finally, the resulting laser bars with 3–8 devices in a row were indium-bonded p-side up onto gold-plated copper heatsinks.

IV. Test and Measurement

A. Experimental Setup

The heatsinks with bonded CCM devices were screwed onto a Peltier-cooled mount on a lateral translation stage allowing easy transition from one device to the next. The devices were tested with one of the two current sources: either continuous wave (CW) or pulsed, with pulses typically 0.8-μs wide and a duty cycle of around 0.3%. Three dc probes were used to bias each device section individually, with the length of the leads minimized to reduce inductive current spikes in the pulsed case. The current through each gain section was controlled either by using both modules of the CW laser driver, or by placing a resistor into one of the probe arms (pulsed case). Output from one facet was coupled into lensed single-mode fiber and fed into an optical spectrum analyzer or a power meter.

To characterize the ML behavior of these devices, intensity autocorrelation studies were performed. The autocorrelator setup illustrated in Fig. 4(a) comprised a Michelson-type interferometer, with one retroreflector mirror positioned on a computer-controlled translation stage and the other one mounted on a loudspeaker. For each step of the translation stage, the loudspeaker was "dithered" at 85 Hz with an amplitude of several wavelengths to average out the fast-varying interferometric fringes. To further minimize the interference effects, the two beams were cross-polarized by inserting a half-wave plate into one of the arms. When the CCM laser was running CW, a chopper was used to trigger the lock-in amplifier measuring the autocorrelation signal; in the pulsed case, the amplifier was locked by the current pulse source itself. All instruments were interfaced with the computer, enabling automatic data acquisition. The computer also maintained constant average optical power throughout each scan by creating a feedback loop between the power meter and the laser driver. A commercial red laser emitting at $\lambda = 670$ nm (*Fuji 670/5S*) was used as a two-photon absorption waveguide detector for the CCM laser wavelength of 860 nm. The red laser was connected directly to the current input of the lock-in amplifier, with no bias applied. When forward biased, the red laser was also instrumental in aligning the setup, which rendered it fully reciprocal with the CCM/red laser as source/detector.

B. Two-Photon Absorption Detector

The use of two-photon absorption in a semiconductor waveguide as a nonlinear detection mechanism for autocorrelation measurements was reported in [19]. The advantages include high sensitivity and a broad wavelength range. One of the drawbacks, however, is the presence of unwanted one-photon absorption (due to donor levels, defects etc.), which leads to a linear component—the photocurrent that is proportionally large at low optical powers—and reduces the height of the correlation peaks

[20]. The measured photocurrent signal S as a function of incident power P can be approximated as

$$S = \alpha P + \beta P^2 \tag{11}$$

with α and β representing the one-and two-photon absorption coefficients, respectively. To characterize the response of the two-photon absorption detector, a power meter was placed in one of the interferometer arms and the $S(P)$ curve was measured for several pump currents above threshold. The curve was then fitted with (11), with the dimensionless ratio β/α^2 taken to be a measure of a detector's nonlinearity. Several red laser-based detectors were tested with a view to selecting those having the highest β/α^2 ratio. The tests revealed that, even in the best devices, the contributions from the linear and nonlinear components were comparable for the power levels used. The upper curve of graph Fig. 4(b) shows the nonlinear response of a detector with $\beta/\alpha^2 \sim 4.8$, measured when the source CCM laser was mode locked. Note that the nonlinearity is apparently larger for the ML case, as the actual peak pulse power is higher than the average power registered by the power meter.

To eliminate the linear component αP from the measured signal, the following calibration procedure was performed immediately before each autocorrelation scan. With the CCM laser running at full power P_0 (whether ML or not), and the translation stage positioned at a delay in between correlation peaks, two detector readings, S_0 and S_1, were taken at powers P_0 and $P_1 = P_0/2$ obtained by placing a 50% filter in the beam, see Fig. 4(b). Assuming the dependence of (11), the linear (αP_0) and quadratic (βP_0^2) terms can be easily found from the two points. The measured autocorrelation data S_k can then be modified by establishing the ratio S_k/S_0 from (11) and correcting it for the linear term. The resulting data are, therefore, normalized to S_0 and approximate the autocorrelation trace that would be registered with a purely quadratic detector. This procedure was found to work accurately only for high peak pulse powers (specifically, for CCM devices mode locked at harmonics $M \leq 7$). Therefore a change in the contrast ratio with and without bias on the saturable absorber (SA) was also registered as evidence of ML. This change was appreciable only when the lasers were driven in pulsed mode, which also helped to maintain lasing stability throughout the scan.

V. Results and Discussion

A. CCM Lasers With Single ICR

The threshold current of CCM lasers typically lay in the range 50–85 mA for a 900-μm-long device, which is 25%–70% higher than in conventional lasers with identical lengths. The optical power was up to 2.2 mW/facet in the CW regime. No reproducible operation was obtained from $m:n$ ratio devices, which exhibited unstable and aperiodic mode spacings. By contrast, the $1:n$ ratio devices manifested the expected increase in spectral mode separation, with a variable number of modes in the spectrum depending on the compound cavity ratio and pumping conditions. Therefore, the results presented in this section were obtained from the $1:n$ ratio devices.

The lasers were ML by applying a negative bias ($V_{SA} = -1$ to -5.5 V) onto the saturable absorber section and adjusting currents through the two gain sections [see Fig. 1(a)] to obtain a spectrum containing evenly spaced modes only. Fig. 5 shows the spectra and corresponding intensity autocorrelation traces for CCM devices ML at different harmonics M of the cavity round-trip frequency. Since the spectrum and autocorrelation are related by a Fourier transform, with higher harmonic numbers the mode separation in the frequency domain can be seen to increase while the delay between consecutive pulses in the time domain becomes shorter. The CCM ML range obtained extends from 131 GHz ($M = 3$) up to 2.1 THz ($M = 33$). In all of these devices, the compound cavity was created by a deep four-slot PBG ICR, as illustrated in Fig. 7(I-a).

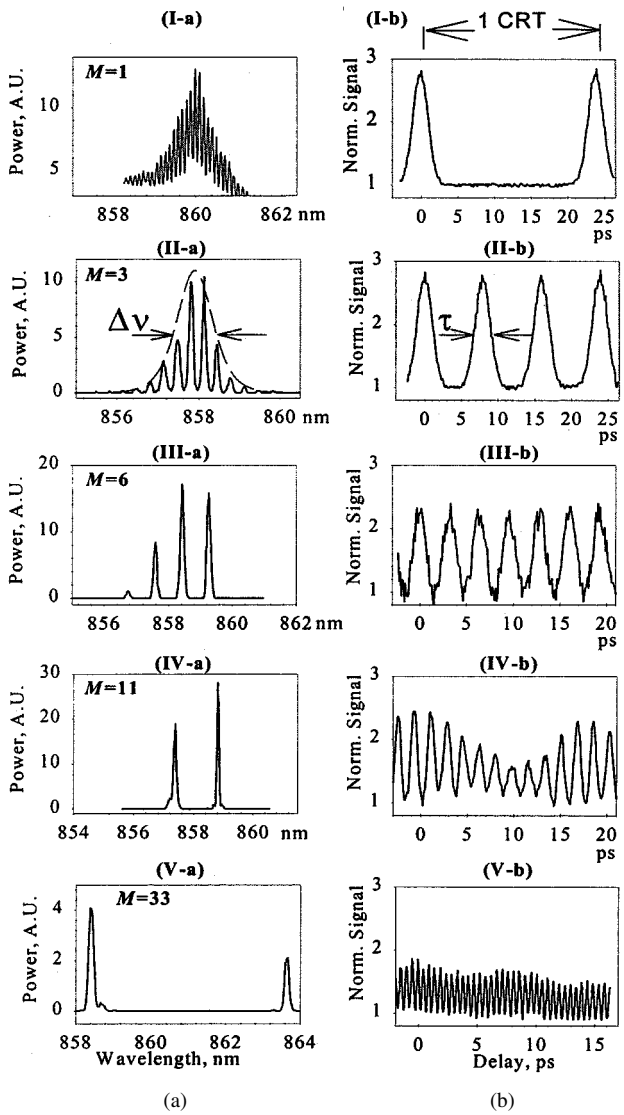

Fig. 5. (a) Spectra and (b) intensity autocorrelation traces for CCM devices ML at different harmonics (M) of the cavity round-trip frequency. To facilitate direct comparison, the horizontal axes in the spectra and autocorrelations are scaled so as to make up for the change in the device length. (I) $M = 1$ (fundamental), $f = 43$ GHz, $\Delta\Lambda = \Delta\lambda_{F-P} = 0.107$ nm, no ICR, cavity length $L = 900$ μm. (II) $M = 3$, $f = 131$ GHz, $\Delta\Lambda = 0.322$ nm, cavity ratio $L_1/L_2 = 300$ μm/600 μm = 1/2. (a) Dashed line shows fitted spectral envelope ($\Delta\nu = 530$ GHz) for assumed pulse shape ($sech^2$) in the transform limit. (b) Autocorrelation peak width $\tau = 1.45$ ps (FWHM) implies actual pulsewidth $\tau_p = 0.95$ ps. (III) $M = 6$, $f = 326$ GHz, $\Delta\Lambda = 0.779$ nm, $L_1/L_2 = 120$ μm/600 μm = 1/5. (IV) $M = 11$, $f = 623$ GHz, $\Delta\Lambda = 1.52$ nm, $L_1/L_2 = 60$ μm/600 μm = 1/10. (V) $M = 33$, $f = 2109$ GHz, $\Delta\Lambda = 5.2$ nm, $L_1/L_2 = 19$ μm/608 μm = 1/32.

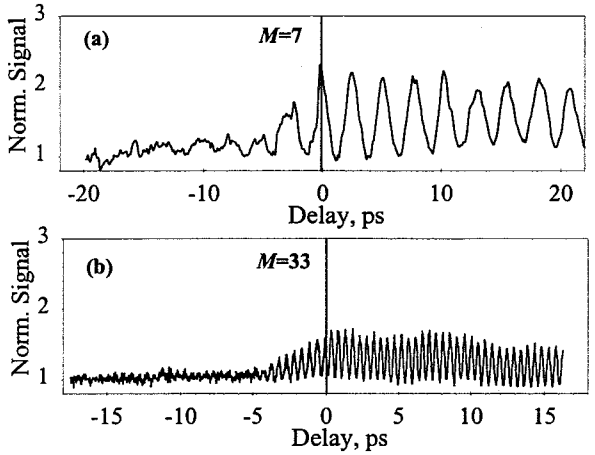

Fig. 6. Proof of ML from intensity autocorrelation: ML trace plotted for positive delays ($\tau > 0$), unlocked for negative delays ($\tau < 0$). Note the change in contrast ratio and coherence time. (a) 7th harmonic device, $f = 396$ GHz, $I_1 = 20.5$ mA; $I_2 = 60$ mA; $\tau > 0$: $V_{SA} = -2.8$ V; $\tau < 0$: $V_{SA} = 0$ V (float). (b) 33rd harmonic device, $f = 2109$ GHz; $\tau > 0$: $V_{SA} = -4$ V; $I_1 = 4.4$ mA; $I_2 = 127$ mA; $\tau < 0$: $V_{SA} = -1.2$ V; $I_1 = 0$ mA (float); $I_2 = 111$ mA.

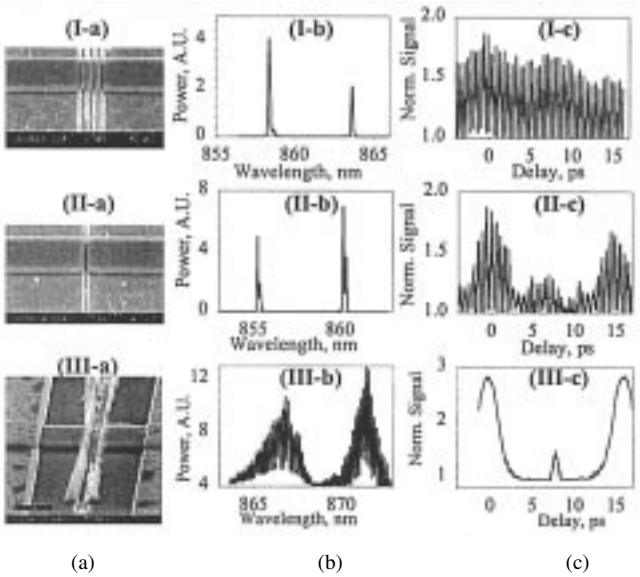

(a) (b) (c)

Fig. 7. SEM photographs of three ICR types with: (a) different reflectivities R_{ICR}; (b) corresponding spectra; and (c) intensity autocorrelation traces for high-harmonic CCM devices. (I) Fourth-order PBG mirror of four deep slots (0.1 -μm-wide $\times$ 2 μm deep), $R_{ICR} \sim 0.7$, $M = 33$. (II) Single deep slot (0.2 μm $\times$ 2 μm), $R_{ICR} \sim 0.08$, $M = 30$. (III) Single shallow "bow-tie" slot (0.4μm $\times$ 0.6 μm), $R_{ICR} \sim 0.001$; $M = 31$.

At the low-frequency end, the plots of Fig. 5(I) and (II) were obtained from a pair of identical-length lasers, as in Fig. 1(b), only one of which had an ICR with a cavity ratio of $L_1 : L_2 = 1 : 2 (M = 3)$. One can see that the CCM laser shows a three-fold multiplication of the mode separation, as well as of the pulse repetition rate (131 GHz against 43 GHz). Pulsewidth was estimated assuming a $sech^2$ pulse shape, which for the spectral envelope of 530 GHz [dashed line in Fig. 5(II-a)] gives a transform-limited pulsewidth of 0.63 ps. This compares with the 0.95-ps pulsewidth inferred from the 1.45–ps-wide autocorrelation peak of Fig. 5(II-b). This discrepancy would suggest that the pulses are chirped, with the pulsewidth being 1.5 times the transform limit. The results are in good agreement with the simulations of Fig. 3(II). Insufficient contrast ratio and number of modes in the spectra preclude meaningful analysis of pulsewidth and modulation depth for higher harmonics, where a reasonable estimate of the pulse duration (FWHM) is $\tau_p \leq 1/2f$, where f is the pulse repetition frequency.

In Fig. 5(III), the harmonic number is further doubled ($M = 6$) by positioning the ICR with a sub-cavity ratio of 1 : 5. Note that since this device is shorter than the previous one, the ML frequency (326 GHz) has more than doubled.

The autocorrelation of the 11th harmonic device of Fig. 5(IV-b) at $f = 623$ GHz contains a slowly-varying envelope at the fundamental ML frequency (~56 GHz) due to the beating of unsuppressed Fabry–Pérot modes inside the two peaks of Fig. 5(IV-a). We believe that this is due to an inaccurate cleaving of the 1 : 10 ratio, which fails to provide a sharp cutoff for the unwanted satellite modes.

Finally, one can count 33 peaks per cavity round-trip in the autocorrelation of Fig. 5(V-b), which corresponds to a pulse repetition frequency of 2.1 THz. As the harmonic ML spectrum consists mainly of two modes [Fig. 5(V-a)] (with a third one suppressed by about 20 dB), the output is essentially a sinusoidally-modulated CW signal. We estimate that the pulsewidth $\tau_p \leq 0.24$ ps (corresponding to a nearly sinusoidal pulse shape).

In these ultrafast devices, the peak pulse power is too small to affect the autocorrelation contrast ratio, and the conclusion as to whether the laser is operating ML or not, can only be drawn by juxtaposing the locked and unlocked cases. The trace of Fig. 6(a) was obtained from a device with $M = 7$, when the bias on the saturable absorber was switched off during the scan as the translation stage was passing through the zero delay position. The trace of Fig. 6(b) was made up of two scans with identical average power but different biases on the absorber for positive and negative delays. In both cases, the correlation peaks can be observed for much longer positive delays than for negative ones. This would indicate a longer coherence time ($\tau_c \gg 1$ cavity round-trip; here, τ_c is defined as the time over which the correlated signal falls to $1/e$ of its value at zero delay [21]), suggesting that the phases of the two modes in Fig. 5(V-a) are locked under the bias conditions used for positive delays. By contrast, the peaks plotted for negative delays fall off very quickly, which suggests random phases with low coherence, or self-pulsing behavior.

B. Effect of ICR Type on High-Harmonic Device Behavior

The behavior of high-harmonic devices ($M > 11$) was highly sensitive to the depth and number of etched ICR slots and bias conditions (see Table I). The lasers having the most reflective ICRs operated single-mode when all sections were forward biased. A second mode would generally appear when one section was reverse biased and currents through the other two were adjusted. In Section III-A, we described the four ICR types fabricated in the CCM devices, as shown in Fig. 7(a). The fourth type, a shallow 13-period grating, appeared to have virtually no effect on the device performance and is therefore not shown. We used a 1-D transfer matrix routine (multilayer stack theory [22]) to estimate the reflectivity R_{ICR} for the first three

TABLE I
BEHAVIOR OF HIGH-HARMONIC DEVICES AS A FUNCTION OF REFLECTOR TYPE AND BIAS CONDITIONS

ICR Type	Estimated Reflectivity	Spectrum (all sections forward biased)	Spectrum (with reverse bias on SA)	Intensity Autocorrelation
4 deep slots	0.7	Single mode	2 harmonic-spaced modes	Near-uniform pulses at harmonic rep. freq.
1 deep slot	0.08	Single mode	2 harmonic-spaced groups of several Fabry-Pérot modes	Pulses at harmonic rep. rate modulated at fundamental freq.
1 shallow slot	0.001	Near single mode	Multiple Fabry-Pérot modes modulated at harmonic spacing	Pulses at fundamental repetition frequency
None	0	Multimode	Broad multimode	Pulses at fundamental repetition frequency

ICR types (the strong coupling case). The computed values are also given in Table I. Note that the actual reflectances are likely to be smaller than the estimates because of the scattering of light at the ICR.

For devices incorporating the most reflective ICR, formed by a deep four-slot PBG mirror [Fig. 7(I-a)] with the estimated $R_{\mathrm{ICR}} \sim 0.7$ (i.e., near the maximum of the spectral selectivity in Fig. 2), all the side modes were suppressed by >15 dB, see Fig. 7(I-b). As a result, the autocorrelation trace of a 33rd harmonic device of Fig. 7(I-c), contains almost no low-frequency modulation. By contrast, where a single deep slot is used with the estimated $R_{\mathrm{ICR}} \sim 0.08$ [Fig. 7(II-a)], the satellite Fabry–Pérot modes are not fully suppressed [Fig. 7(II-b)], and the pulses of [Fig. 7(II-c)] are strongly modulated at the fundamental cavity round-trip frequency. Finally, a single shallow slot with $R_{\mathrm{ICR}} \sim 0.001$ in a 1 : 30 ratio device [Fig. 7(III-a)] only causes low-depth spectral modulation as shown in Fig. 7(III-b). The autocorrelation trace of Fig. 7(III-c) indicates only fundamental frequency ML and contains no visible high-frequency components. It can therefore be concluded that highly reflective ICRs are required for subharmonic-free ML of these ultrahigh-frequency devices.

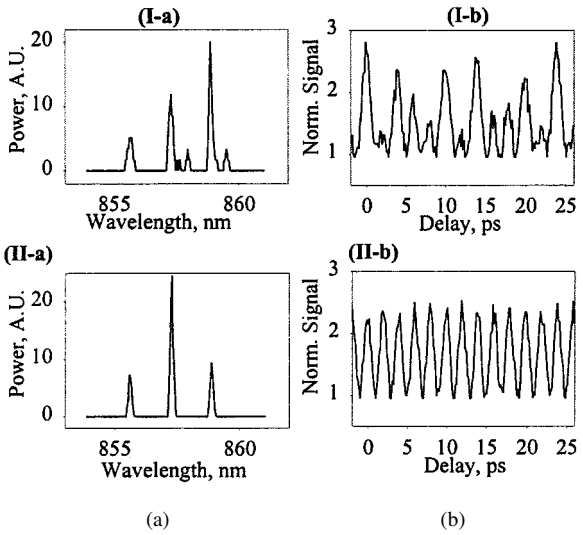

Fig. 8. (a) Experimental spectra and (b) intensity autocorrelation traces of 12th harmonic CCM devices ($M = 12$, $f = 504$ GHz, $\Delta\Lambda = 1.29$ nm). (I) Single deep slot at 5/12 of the cavity length ($L_1/L_2 = 375\ \mu$m/525 μm = 5/7), $R_{\mathrm{ICR}} \sim 0.08$. (II) Twin slots with $R_{\mathrm{ICR}} \sim 0.08$ each, positioned at 5/12 and 1/3 of the cavity length.

C. CCM Lasers With Twin ICR

In [16], the use of multiple ICRs was proposed with a view to improving side-mode suppression for single-mode operation. Here, we developed this idea to create a device with two ICRs at specific locations to obtain a side mode-free harmonic spectrum (and unmodulated pulses) with relatively small ICR reflectivities. A theoretical discussion of this idea was presented in the last two paragraphs of Section II.

A pair of same-length CCM lasers was fabricated, with one having a 5 : 7 ICR only, and the other one having both a 5 : 7 and a 1 : 2 ICR. The total cavity length was 900 μm. The type of reflector used for both ICRs was that of Fig. 7(II-a) (single deep slot), which has already been shown to be inadequate for modulation-free ML in the single-ICR configuration. The spectrum of the 5 : 7 ICR-only laser [Fig. 8(I-a)] does indeed contain residual Fabry–Pérot modes between the harmonic ones, resulting in a highly ambiguous autocorrelation, see Fig. 8(I-b). The other device, having both slots, exhibits a spectrum free of side-modes [Fig. 8(II-a)] and a modulation-free autocorrelation at $f = 504$ GHz [Fig. 8(II-b)]. These results are in good agreement with the theoretical simulations of a similar structure, shown in Fig. 3(IV) and (V). Because the dual-ICR laser

contains fewer slots, it also has a threshold current 12% lower than that of a PBG ICR device.

We believe that the twin-ICR approach allows more accurate selection of the desired harmonic number than the single slot approach, as the relative position of the two ICRs is defined lithographically. On the other hand, it lacks the flexibility of the single-ICR layout, which allows the harmonic number to be chosen at the cleaving stage.

VI. Conclusion

We have reported the successful realization of the type of ultrafast semiconductor laser proposed theoretically in [4], [9], [10], based on the harmonic CCM model. To achieve harmonic operation, we have fabricated devices incorporating a novel compound cavity configuration with the use of highly reflective PBG microstructures. These lasers were cleaved to different lengths to form compound cavities of varying asymmetry, which defined the harmonics of the fundamental round-trip frequency at which the devices were expected to modelock.

Autocorrelation studies confirmed ML operation at selected harmonic numbers from 3 to 33, with corresponding repetition frequencies from 131 GHz up to a record high of 2.1 THz. To our knowledge, this is the highest ML frequency achieved from a semiconductor laser or, indeed, any type of laser. This demonstrates the suitability of the CCM technique for the generation of microwave-modulated optical power in the terahertz range. With the optical power concentrated mainly in two dominant modes, these lasers should be particularly suitable for local oscillator applications where a sinusoidal output is desired.

We have also investigated device behavior for different reflector types and reflectivities. We have found that subharmonic-free ML operation of the high-harmonic devices required highly reflective ($R_{\mathrm{ICR}} \sim 0.7$) PBG-based ICRs.

Finally, we have engineered a twin-reflector CCM laser by an appropriate choice of the two ICR positions. Mode locked at 504 GHz, this laser has a lower threshold current than a four-slot PBG device of the same length. This approach is probably most suitable for devices designated for a specific harmonic number and ML frequency at the design stage.

References

[1] E. R. Brown, F. W. Smith, and K. A. McIntosh, "Coherent millimeter-wave generation by heterodyne conversion in low-temperature-grown GaAs photoconductors," *J. Appl. Phys.*, vol. 73, p. 1480, 1993.

[2] K. A. McIntosh, E. R. Brown, K. B. Nichols, O. B. McMahon, W. F. DiNatale, and T. M. Lyszczarz, "Terahertz photomixing with diode lasers in low-temperature-grown GaAs," *Appl. Phys. Lett.*, vol. 67, no. 26, p. 3844, 1995.

[3] E. L. Portnoi, B. B. Gorfinkel, E. A. Avrutin, I. G. Thayne, D. A. Barrow, J. H. Marsh, and Y. Li, "Optoelectronic microwave-range frequency mixing in semiconductor lasers," *IEEE J. Sel. Top. Quantum Electron.*, vol. 1, no. 2, p. 451, 1995.

[4] E. A. Avrutin, J. H. Marsh, and E. L. Portnoi, "Monolithic and multi-gigahertz mode-locked semiconductor lasers: Constructions, experiments, models and applications," *Proc. IEE Optoelectron.*, vol. 147, p. 251, 2000.

[5] E. L. Portnoi and A. V. Chelnokov, "Passive mode-locking in a short-cavity laser," in *Dig. 12th IEEE Semiconductor Conf.*, Davos, Switzerland, 1990, pp. 140–141.

[6] J. F. Martins-Filho, E. A. Avrutin, C. N. Ironside, and J. S. Roberts, "Monolithic multiple colliding pulse mode locked quantum well lasers: Experiment and theory," *IEEE J. Select. Topics Quantum Electron.*, vol. 1, pp. 539–552, 1995.

[7] T. Shimizu, I. Ogura, and H. Yokoyama, "860 GHz rate asymmetric colliding pulse modelocked diode lasers," *Electron. Lett.*, vol. 33, p. 1868, 1997.

[8] S. Arahira, Y. Matsui, and Y. Ogawa, "Mode-locking at very high repetition rates more than terahertz in passively mode-locked distributed-Bragg-reflector laser diodes," *IEEE J. Quantum Electron.*, vol. 32, p. 1211, July 1996.

[9] E. A. Avrutin, J. H. Marsh, and J. M. Arnold, "Modeling of semiconductor laser structures for passive harmonic mode locking at terahertz frequencies," *Int. J. Optoelecron.*, vol. 10, p. 427, 1995.

[10] E. A. Avrutin, J. H. Marsh, J. M. Arnold, T. F. Krauss, H. Pottinger, and R. M. De La Rue, "Analysis of harmonic (sub) THz passive mode-locking in monolithic compound cavity Fabry–Pérot and ring laser diodes," *Proc. IEE Optoelectron.*, vol. 146, p. 55, 1999.

[11] E. A. Avrutin, J. H. Marsh, and J. M. Arnold, "Static and dynamic modal analysis of monolithic mode-locked semiconductor lasers," in *Proc. 12th LEOS Annual Mtg.*, San Francisco, CA, Nov. 1999, paper CThF4.

[12] E. A. Avrutin, B. D. Allen, R. M. DeLaRue, J. H. Marsh, J. M. Arnold, M. Izutsu, J. S. Aitchison, and T. F. Krauss, *Proc. Dig. CLEO-Europe*, Glasgow, U.K., Sept. 1998, p. 278.

[13] C. H. Henry and R. F. Kazarinov, "Stabilization of single frequency operation of coupled cavity lasers," *IEEE J. Quantum Electron.*, vol. QE-20, pp. 733–744, July 1982.

[14] L. A. Coldren, B. I. Miller, K. Iga, and J. A. Rentschler, "Monolithic two-section GaAsP/InP active-optical-resonator devices formed by reactive ion etching," *Appl. Phys. Lett.*, vol. 38, no. 5, pp. 315–318, 1981.

[15] L. F. Dechiaro, "Spectral width reduction in multi-longitudinal mode lasers my spatial loss profiling," *J. Lighwave Technol.*, vol. 9, pp. 975–989, 1991.

[16] D. A. Kozlowski, J. S. Young, J. M. C. England, and R. G. S. Plumb, "Longitudinal mode control in 1.3 mm Fabry–Pérot lasers by mode suppression," *Proc. Optoelectron.*, vol. 143, no. 1, pp. 71–76, 1996.

[17] T. F. Krauss and R. M. De La Rue, "Optical characterization of waveguide based photonic microstructures," *Appl. Phys. Lett.*, vol. 68, no. 12, pp. 1613–1615, 1996.

[18] T. F. Krauss, B. Vögele, and R. M. De La Rue, "Waveguide microcavity based photonic microstructures," *IEEE Photon. Technol. Lett.*, vol. 9, pp. 176–178, 1997.

[19] F. R. Laughton, J. H. Marsh, D. A. Barrow, and E. L. Portnoi, "The two photon absorption semiconductor waveguide autocorrelator," *IEEE J. Quantum Electron.*, vol. 30, pp. 838–845, 1994.

[20] M. M. Karkhanehchi, D. A. Barrow, A. C. Bryce, C. J. Hamilton, and J. H. Marsh, "The influence of single-photon absorption on the performance of the two-photon waveguide autocorrelator," *IEEE J. Quantum Electron.*, vol. 33, p. 933, June 1997.

[21] L. Mandel and E. Wolf, "The measures of bandwidth and coherence time in optics," *Proc. Mod. Phys.*, vol. 80, pp. 894–897, 1962.

[22] T. Tamir, *Guided-Wave Optoelectronics*. New York: Springer, 1990, pp. 43–50.

[23] E. A. Avrutin, J. H. Marsh, and J. M. Arnold, "Static and dynamic modal analysis of monolithic mode-locked semiconductor lasers," *J. Appl. Phys.*, submitted for publication.

Dan A. Yanson was born in Leningrad, U.S.S.R., in 1973. He received the M.Sc. degree in optoelectronic systems from the Electrical Engineering University, St. Petersburg, Russia, in 1996. He then joined the Integrated Optics Laboratory, Ioffe Physico-Technical Institute, St Petersburg, Russia. He is currently working toward the Ph.D. degree with the Optoelectronics Research Group, University of Glasgow, Glasgow, U.K.

His research interests include ultrafast diode lasers and design and fabrication of III–V semiconductor optoelectronic devices.

Michael W. Street was born in Belfast, Northern Ireland, U.K., in 1969. He received the M.Eng. degree in electrical and electronics engineering from Imperial College, University of London, London, U.K., in 1993, and the Ph.D. degree in electronics from the University of Glasgow, Glasgow, U.K., in 1997. His doctoral research was concerned with quantum-well intermixing for the control of second-order nonlinear optical effects in GaAs–AlGaAs multiple-quantum-well waveguides.

His postdoctoral work has been in the field of mode-locked semiconductor lasers for the generation and conversion of terahertz frequencies. He is currently with Alcatel Optronics, Livingston, U.K.

Stewart D. McDougall was born in Scotland, U.K., in 1972. He received the first-class B.Eng. (Hons.) degree in physics and electronic engineering in 1993 and the Ph.D. degree in optoelectronics in 1997, both from the University of Glasgow, Glasgow, U.K. His Ph.D. research involved work on high-repetition mode-locking of quantum-well semiconductor lasers and was a CASE studentship with BT Laboratories Martelsham Heath, U.K.

He was then a Research Assistant in the Optoelectronics Research Group, Department of Electronics and Electrical Engineering, University of Glasgow, where he was involved in the development of long-wavelength mode-locked semiconductor lasers, quantum-well intermixing techniques, and high-speed photodetectors. He is currently an Engineering Manager with Intense Photonics, Glasgow, U.K., responsible for development of 980-nm lasers.

Iain G. Thayne (M'00) is an EPSRC Advanced Research Fellow and Senior Lecturer in the Department of Electronics and Electrical Engineering, University of Glasgow, Glasgow, U.K., where he leads the Ultrafast Systems Group. He previously worked for Philips Research Labs and Norwegian Telecom. His research interests include the design, fabrication, characterization, and integration of a wide range of millimeter-wave electronic and optoelectronic components. He has (co)-authored over 80 refereed journal and conference papers.

Since 2000, Dr. Thayne has been a member of the IEEE U.K. and Republic of Ireland Administrative Committees for the joint chapters on IEEE MTT, EDS, APS, and LEOS and the Communications Society chapter.

John H. Marsh (M'91–SM'91–F'00) is the Chief Research Officer of Intense Photonics Ltd, Glasgow, U.K., a company he co-founded in 2000. He is currently seconded to Intense Photonics from the University of Glasgow, Glasgow, U.K., where he holds the post of Professor of Optoelectronic Systems in the Department of Electronics and Electrical Engineering. His research interests are particularly concerned with linear and nonlinear integrated optoelectronic systems. He has developed new integration technologies for photonic integrated circuits based on quantum-well devices and quantum-well intermixing, and has built up an extensive program of work at the University of Glasgow on III-V based photonic integrated circuits for high-speed digital optical communications. He is author or co-author of more than 300 journal and conference papers.

Dr. Marsh is a Fellow of the Institution of Electrical Engineers (FIEE), the Royal Society of Arts (FRSA), and the Royal Society of Edinburgh (FRSE). He is a member of the IEEE Lasers and Electro-Optics Society (LEOS), IEEE Electron Devices Society (EDS), IEEE Communications Society and the Optical Society of America. He is currently a member of the LEOS Optoelectronic Materials and Processing Technical Committee and of the EDS Optoelectronic Devices Technical Committee. From 1996 to 1998, he was Founding Chair of the Scottish Chapter of LEOS. Since 1999, he has been LEOS Vice President Membership and Regional Activities for Europe, the Mid-East, and Africa. He was an Elected Member of the LEOS Board of Governors for three years, commencing January 2001. He is a member of the Executive Team of the IEE Photonics Network, the Engineering and Physical Sciences Research Council's Electronic and Photonic Technologies College, and of the Council of the Scottish Optoelectronics Association.

Eugene A. Avrutin (M'95) was born in St. Petersburg, U.S.S.R., in 1963. He received the M.Sc. degree (with distinction) from St. Petersburg Technical University (then Leningrad Polytechnical Insitute), St. Petersburg, U.S.S.R., in 1986, and the Ph.D. degree from A.F. Ioffe Physico-Technical Institute, St. Petersburg, Russia, in 1994.

From 1986 to 1993, he was with the Integrated Optics Laboratory, Ioffe Physico-Technical Institute, St Petersburg, Russia, working mainly on the theory and modeling of spectral, dynamic, and polarization properties of advanced semiconductor lasers. This work included an exchange fellowship in 1992, spent at the Department of Electronic and Electrical Engineering, University of Bath, Bath, U.K. From 1994 to 1999, he was with the Department of Electrical and Electronic Engineering, University of Glasgow, Glasgow, U.K., where his research centered on theoretical and numerical analysis of ultrafast diode lasers and new materials for semiconductor optoelectronics. He is currently a member of staff at the Department of Electronics, University of York, York, U.K., where his research interests are the theory, modeling, and design of optoelectronic devices and the advancement of CAD techniques for photonics.